



Initial Post Irradiation Examination of Irradiated Yttrium Hydride

August 2022

Changing the World's Energy Future

M. Nedim Cinbiz
Joey A. Charboneau
Ian M. Hobbs
Glen C. Papaioannou
Thomas A. Johnson
Lance A. Hone
Scott C. Middlemas
Chase N. Taylor



DISCLAIMER

This information was prepared as an account of work sponsored by an agency of the U.S. Government. Neither the U.S. Government nor any agency thereof, nor any of their employees, makes any warranty, expressed or implied, or assumes any legal liability or responsibility for the accuracy, completeness, or usefulness, of any information, apparatus, product, or process disclosed, or represents that its use would not infringe privately owned rights. References herein to any specific commercial product, process, or service by trade name, trade mark, manufacturer, or otherwise, does not necessarily constitute or imply its endorsement, recommendation, or favoring by the U.S. Government or any agency thereof. The views and opinions of authors expressed herein do not necessarily state or reflect those of the U.S. Government or any agency thereof.

Initial Post Irradiation Examination of Irradiated Yttrium Hydride

**M. Nedim Cinbiz
Joey A. Charboneau
Ian M. Hobbs
Glen C. Papaioannou
Thomas A. Johnson
Lance A. Hone
Scott C. Middlemas
Chase N. Taylor**

August 2022

**Idaho National Laboratory
Idaho Falls, Idaho 83415**

<http://www.inl.gov>

**Prepared for the
U.S. Department of Energy
Office of Nuclear Energy
Under DOE Idaho Operations Office
Contract DE-AC07-05ID14517**

Page intentionally left blank

SUMMARY

Yttrium hydride (YH_x) is considered as a candidate neutron moderator component for high-temperature micro nuclear reactors (microreactors). While thermophysical and thermodynamics data is present for unirradiated YH_x , properties of neutron irradiated YH_x are limited. Therefore, Department of Energy (DOE) Office of Nuclear Energy (NE) Micro Reactor Program (MRP)'s technology maturation work scope initiated a comprehensive irradiation campaign and following post irradiation examination (PIE) of YH_x . Irradiations of YH_x specimens of various geometries and titanium-zirconium-molybdenum (TZM) sheets were performed in the Advanced Test Reactor (ATR) at Idaho National Laboratory (INL) at temperatures of 600, 700, and 800°C. A total of 102 YH_x specimens, 36 TZM sheets, and passive instrumentation, were encapsulated in 6 TZM capsules. Capsules were irradiated in ATR for two months (60 full power days). Irradiation commenced February 19, 2021, and completed April 19, 2021. Samples were transported to Idaho National Laboratory's (INL's) Hot Fuels Examination Facility (HFEF) on June 16, 2021. The irradiation assembly was disassembled October 6, 2021.

This report describes the initial PIE activities of neutron irradiated YH_x and critical method development for hydrogen content measurements. This report is organized as follows. A brief description of the ATR irradiation and specimens is presented. Secondly, the PIE methods applied during this fiscal year (FY) were concisely described. This is followed by the status of the PIE and initial examination results. In addition, an alternative method for hydrogen content measurements in metal hydrides is described. Finally, main outcomes of PIE activities and future work are reported.

Based on the initial PIE results, (i) the TZM capsules and most of the YH_x specimens maintained their geometrical stability after the ATR irradiation, (ii) a large number of samples appear to have not underwent hydrogen redistribution even at 800°C, as observed in neutron radiography, (iii) a severe interaction or redistribution occurred in a limited number of YH_x specimens, observed as a decolorization of YH_x , and (iv) thermal stability of YH_x was confirmed for fresh and irradiated specimens at temperatures up to 800°C.

To summarize, initial PIE results are significantly improving the current understanding and available data for neutron irradiated YH_x for high temperature moderator applications. With the upcoming completion of PIE from this campaign, solid conclusions are expected that will support the technological maturation of hydride-moderated microreactors.

ACKNOWLEDGEMENTS

Authors are thankful to the Materials and Fuel Complex's supporting staff for the PIE activities and specimen transfers. Authors are indebted to Cad Christensen and John Stanek for the retrieval of the specimens from irradiation vehicles at HFEF. Authors also acknowledge Richard Farrar who enabled critical PIE activities at the Analytical Laboratory. Authors thank to Larry Greenwood from Pacific Northwest National Laboratory for conducting fluence wire examinations.

Page intentionally left blank

CONTENTS

SUMMARY	iv
ACKNOWLEDGEMENTS.....	v
ACRONYMS	xi
1. INTRODUCTION	1
2. SUMMARY OF ATR IRRADIATIONS	1
3. POST IRRADIATION EXAMINATION METHODS.....	4
3.1 Neutron radiography.....	4
3.2 Fluence wire examinations	6
3.3 Melt wire examinations	6
3.4 Optical Inspection of Samples.....	6
3.5 Mass, volume, and density measurements.....	7
3.6 Thermal diffusivity	8
4. STATUS OF THE YH _x PIE.....	8
5. PIE RESULTS	9
5.1 Neutron radiography.....	9
5.2 Specimen retrieval and transfer	11
5.3 Fluence wires.....	13
5.4 Melt wires.....	14
5.5 Optical inspection of YH specimens	16
5.6 Mass, volume, and density measurements of YH _x	22
5.7 Thermal diffusivity results.....	24
6. DEVELOPMENT HYDROGEN MEASUREMENT TECHNIQUE BY INERT GAS FUSION (IGF).....	25
7. CONCLUSIONS AND FUTURE WORK.....	29
8. REFERENCES	31

FIGURES

Figure 1. Schematics of specimen stacking in a TZM capsule. Green: YH_x and orange: TZM (not to scale).	2
Figure 2. Calculated capsule design temperatures and the calculated fast-fluence distribution	3
Figure 3. Schematics of the indirect transfer method for neutron radiography. Components are not depicted in actual scale.....	4
Figure 4. Neutron radiography setup for the LANL-MOD1A ATR Basket	5
Figure 5. Stage Micrometer KR-812 as imaged on Dino-Lite AM73915MZTL digital microscope.	7
Figure 6. Micrometrics AccuPyc II 1345 gas displacement pycnometer.....	7
Figure 7. (a), Yttrium sample, centering cone holder, and mask (b) The yttrium hydride disc placed on the holder, (c) LFA test set-up with sample loaded.....	8
Figure 8. Neutron radiography of the ATR fixture and LANL capsule and YH_x specimens at angles of 0, 120, and 240°	10
Figure 9. Neutron radiographs of individual capsules at angle of 240°	11
Figure 10. (a) LANL capsule sectioning (b) cracking of LANL capsule, and (c) sectioned capsule with specimens	12
Figure 11. (a) Powdered and (b) ruptured specimens.....	12
Figure 12. Axial profile of the neutron fluence based on fluence wire analysis	14
Figure 13. Photographs of melt wires from capsules 1 (a and b) and 4 (c and d)	15
Figure 14. Photographs of melt wires from capsules 2B (a and b) and 5 (c and d)	15
Figure 15. Photographs of melt wires from capsules 3A (a and b) and 6 (c and d)	15
Figure 16. Percent variation of specimen masses after irradiation.....	23
Figure 17. Percent variation of specimen volumes after irradiation.....	24
Figure 18. Percent variation of specimen density after irradiation.....	24
Figure 19. Mean thermal diffusivity ($\text{mm}^2 \text{s}^{-1}$) as a function of temperature for a fresh yttrium hydride disc as well as two irradiated yttrium hydride discs from capsule #2B ($T_{\text{irr}}=700^\circ\text{C}$).....	25
Figure 20. Process of YH_x dilution process for IGF analysis.....	26

TABLES

Table 1. Expected average temperature of the LANL capsules, assuming cracked capsule was filled by air.	4
Table 2. Status of the specimen after capsule opening.....	13
Table 3. Fluences levels on the fluence wires as calculated and measured.....	14
Table 4. Melt wire examination results	16
Table 5. Optical pictures of powder metallurgy manufactured YH_x , irradiated at 600°C	17
Table 6. Optical pictures of massively hydrided YH_x , irradiated at 600°C	18
Table 7. Optical pictures of powder metallurgy manufactured YH_x , irradiated at 700°C	19
Table 8. Optical pictures of massively hydrided YH_x , irradiated at 700°C	20
Table 9. Optical pictures of powder metallurgy manufactured YH_x , irradiated at 800°C	21
Table 10. Optical pictures of massively hydrided YH_x , irradiated at 800°C	22
Table 11. Hydrogen content of yttria powder specimens as measured by IGF.....	27
Table 12. Mass measurements of yttria, YH_x , and mixture specimens	28
Table 13. Hydrogen content measurements of mixture, YH_x , and back calculated bulk YH_x , and stoichiometry ratio (H:Y).....	28

Page intentionally left blank

ACRONYMS

AL – Analytical Laboratory
ASTM – American Society of Testing and Materials
ATR – Advanced Test Reactor
DOE – Department of Energy
DSC – differential scanning calorimetry
FY – fiscal year
GDOES – glow discharge optical emission spectroscopy
HFEF – Hot Fuels Examination Facility
IGF – inert gas fusion
INL – Idaho National Laboratory
LANL – Los Alamos National Laboratory
LEGe – low energy germanium
LFA – laser flash analysis
MFC – Materials and Fuels Complex
MRP – Micro Reactor Program
NE – Nuclear Energy
NIST – National Institute of Standards and Technology
NRAD – Neutron Radiography Reactor
PIE – post irradiation examination
PNNL – Pacific Northwest National Laboratory
RUS – resonant ultrasound spectroscopy
SiC – silicon carbide
TEM – transmission electron microscopy
TZM – titanium zirconium molybdenum
XRD – x-ray diffraction
YH_x – yttrium hydride

Page intentionally left blank

Initial Post Irradiation Examination of Irradiated Yttrium Hydride

1. INTRODUCTION

The Department of Energy (DOE) Office of Nuclear Energy (NE) Micro Reactor Program (MRP) aims to mature critical technologies which enable the deployment of microreactors [1]. Microreactors are considered to operate at low power (<20MW thermal) and high temperatures (>600°C). The main design features of these reactors are being plug-and-play, integrally safe, and truck-transportable with current road infrastructure[1]. Transportability necessitates significant volume and mass reduction of the nuclear reactor which can be achieved by incorporating solid neutron moderators bearing light-weight elements, such as hydrogen, carbon, and beryllium [2, 3]. Among these, hydrogen can efficiently slow down fast neutrons to thermal energies. Therefore, hydrogen bearing solid materials, like metal hydrides, are potential candidates for neutron moderators in microreactors.

For neutron moderator applications, yttrium hydride (YH_x , x stands for hydrogen stoichiometry) is considered because of its high hydrogen retention capability and thermal stability [3, 4]. While basic thermodynamic and thermophysical data are present for fresh YH_x [5-14], post-irradiation examination (PIE) data are inadequate [4, 15] to support the deployment of microreactors. To establish a materials qualification strategy for the solid moderators, PIE must show whether, or to what extent, neutron irradiation impacts the solid moderator's form and function. Thus, the effect of irradiation on the critical material properties, as well as the dimensional stability, must be determined for irradiated YH_x to serve as the basis for the solid moderator qualification and to inform microreactor performance and safety codes. Thus, MRP's technology maturation work scope initiated a comprehensive campaign which involves YH_x solid moderator fabrication and subsequent neutron irradiations at microreactor relevant temperatures.

Irradiations were performed in the B2 position in the Advanced Test Reactor (ATR) at Idaho National Laboratory (INL). A total of 102 YH_x specimens and 36 titanium-zirconium-molybdenum (TZM) sheets, including passive instrumentation (12 melt and 3 fluence wires, and 6 silicon carbide (SiC) sticks) were encapsulated in 6 TZM capsules, and these 6 capsules were irradiated in ATR for two months (60 full power days). Irradiation commenced February 19, 2021 and completed April 19, 2021. Samples were transported to Idaho National Laboratory's (INL's) Hot Fuels Examination Facility (HFEF) on June 16, 2021. The irradiation assembly was disassembled October 6, 2021, after which PIE commenced. PIE activities included non-destructive and destructive characterizations of YH_x as reported in the YH_x PIE plan [16].

This report describes the first half of PIE and related activities completed for solid YH_x through fiscal year 2022 (FY22). Neutron radiography of the irradiated assembly was the first PIE activity to be performed. After the neutron radiography, the irradiated specimens were retrieved from each of the irradiation capsules in the HFEF hot cell. All specimens were catalogued, and each specimen was contained in a metal container with specific serial number to maintain material identity. Fluence wires were packaged and shipped to Pacific Northwest National Laboratory (PNNL) for examinations. Other passive instrumentation specimens, SiC thermometry sticks and melt wires were also sent to INL's relevant facilities for examinations. YH_x specimens were transferred to INL's Analytical Laboratory (AL) in groups due to radiological dose limitations of the facility. Basic PIE activities of optical inspections, mass, volume, and density measurements were performed at AL. After completing basic PIE, thermal diffusivity measurements were commenced on selected specimens. Additionally, an analytical measurement process was developed to assess hydrogen content of the irradiated YH_x specimens.

2. SUMMARY OF ATR IRRADIATIONS

LANL moderator irradiations were drop-in experiments with no active instrumentation. The irradiation campaign aimed to investigate the irradiation performance YH_x that was manufactured via powder metallurgy and massive hydriding. Estimated irradiation temperatures were nominally 600, 700,

and 800°C based on vertical position in the reactor. Cylindrical YH_x specimens were inserted into TZM capsules which were weld sealed. After assembly, one TZM capsule was identified as having a hairline crack, initially originated at the weld location, partially propagated along the capsule height; the decision to proceed with irradiations was made by the program. Each TZM capsule (hereafter referred to as the LANL capsule) contained 17 YH_x specimens, 6 TZM sheets, and 1 TZM ring. Melt wires were inserted inside TZM ring. YH fabrication and the LANL capsule assembly was performed at LANL. LANL capsules were shipped to INL and placed within a clamshell fixture and ATR basket. Two LANL capsules were contained in one clamshell and two fluence wires and one SiC passive temperature monitor were located in the center of each clamshell. In total, 6 TZM capsules containing 102 YH_x specimens were irradiated, for detailed information see [16]. YH_x specimens were identified as resonant ultrasound spectroscopy (RUS), glow discharge optical emission spectroscopy (GDOES), transmission electron microscopy (TEM), laser flash analysis (LFA), and differential scanning calorimetry (DSC).

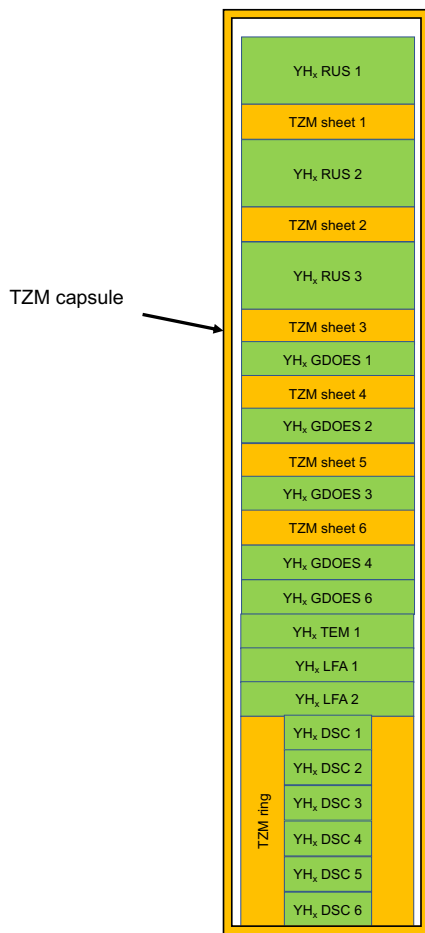


Figure 1. Schematics of specimen stacking in a TZM capsule. Green: YH_x and orange: TZM (not to scale).

LANL capsules 1, 2B, and 3A contained powder metallurgy samples to be irradiated at 600, 700, and 800°C, respectively. LANL capsules 4, 5, and 6 contained direct hydride YH_x samples irradiated at the 600, 700, and 800°C, respectively. The nominal average design temperature of each LANL capsule and the distribution of calculated fast fluence are shown in Figure 2. The average temperature of capsules 1

and 4 were estimated as 600°C; 700°C for capsules 3A and 6; and capsules 2B and 5 were estimated at 800°C. The fast neutron fluence had a skewed cosine shape and was calculated in the range of 1.05-1.25 10^{21} n/cm². Specimens in capsules 1 and 4 were subjected to relatively fewer neutrons during the drop-in irradiations. Capsules 3A and 6 were subject to constant fluence as well.

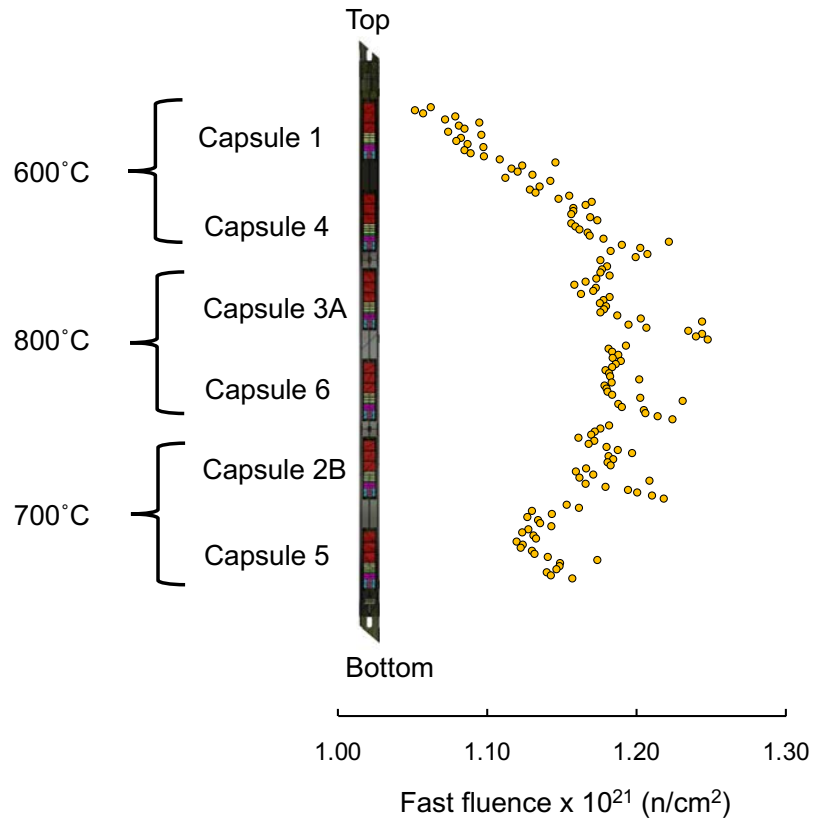


Figure 2. Calculated capsule design temperatures and the calculated fast-fluence distribution

As noted above, capsule 2B had a crack at its weld location and this was reported in [16]. The effect of this condition was simulated in the thermal calculations where the internal gas of LANL capsule 2B was replaced by air to mimic the worst conditions (conservative approach). The consequence of this gas exchange would result in a higher irradiation temperature (769°C instead of 700°C). The expected average temperatures of the capsules is shown in Table 1. For intact capsules, the temperature increased by 10°C in comparison to a temperature increase of 69°C for capsule 2B.

Table 1. Expected average temperature of the LANL capsules, assuming cracked capsule was filled by air.

Capsule #	Expected Temperature (°C)
1	609
4	610
3A	811
6	813
2B	769
5	715

3. POST IRRADIATION EXAMINATION METHODS

FY22 PIE activities included non-destructive and destructive characterizations of specimens. These included visual examinations and neutron radiography of the ATR basket, visual examinations of each capsule, specimen retrieval and cataloging, examination of passive instrumentation, optical inspection, basic physical property measurements (mass, volume, and density), and initiation of preliminary thermal property measurements. Specific PIE methods are briefly described in the following sections.

3.1 Neutron radiography

Neutron radiography uses the indirect transfer method which provides higher spatial resolution in the radiographic image. The working principal of the indirect transfer method (see Figure 3) is as follows. The incoming neutrons from the reactor initially penetrate through the sample, and the transmitted neutrons are shined onto a cassette where dysprosium (Dy), cadmium (Ca), and indium (In) foils are inserted, respectively. Dy and In foils are used for thermal and epithermal neutron imaging while Ca foil is for filtering thermal neutrons for epithermal imaging. After cassette irradiation, Dy and In become temporarily radioactive by emitting positively or negatively charged electrons (β decay). Neutron-exposed Dy and In foils are then placed onto an electron sensitive x-ray film in a darkroom. Foils and x-ray films were kept in contact for five half-lives of β decay for Dy and In (~ 8 hours). The image of the sample is formed via electron-stimulated chemical reactions in the X-ray film. Images formed in the film have $\sim 200 \mu\text{m}$ resolution.

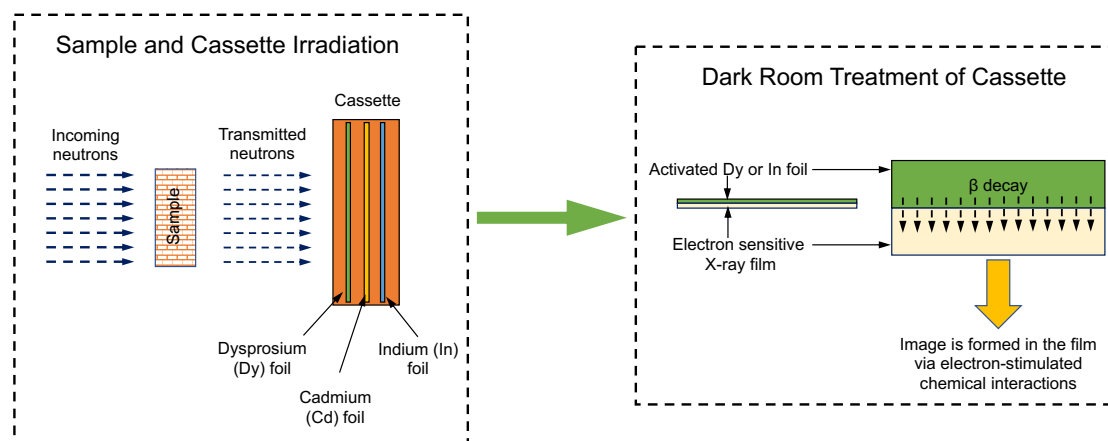


Figure 3. Schematics of the indirect transfer method for neutron radiography. Components are not depicted in actual scale.

Neutron radiography of the ATR basket was performed at the East Radiography Station of the Neutron Radiography Reactor (NRAD) at HFEF. The ATR basket was hung inside in an aluminum carrier, and a ruler was placed on the carrier for capsule measurements during radiography (see Figure 4). The graduations on the ruler were filled with gadolinium, a neutron absorber, allowing the numbers and graduations to show up in the image. The ATR basket was imaged at two elevations with 190.5 mm (7.5") overlap and three orientations of 0, 120, and 240° by manual remote rotation. Neutron exposure time was 22 minutes per shot. After neutron exposure and radiation survey, the cassette was transferred to the darkroom for the x-ray film treatment. Dy and In foils were removed from the irradiation cassette. Foils were then placed onto x-ray films in separate cassettes that were connected to a vacuum system. The vacuum was utilized to provide close contact of foils and films. A double emulsion very-fine grain Carestream Industrex T200 and single emulsion ultra-fine grain AGFA D3SC x-ray films were used for In and Dy foils, respectively. Films were subjected to β radiation from irradiated foils for five half-lives^a. After this period, the x-ray films were removed from the cassette and treated using a Kodak M35A automatic film processor. Developed films were then digitized to 1200 dpi and 16-bit Tagged Image File Format (TIFF) using a Fuji FineScan 2750 flatbed scanner. In addition to ATR basket experiment, a "resolution test piece" was also subjected to the neutron radiography and the film treatment to determine optical quality and resolution of films.

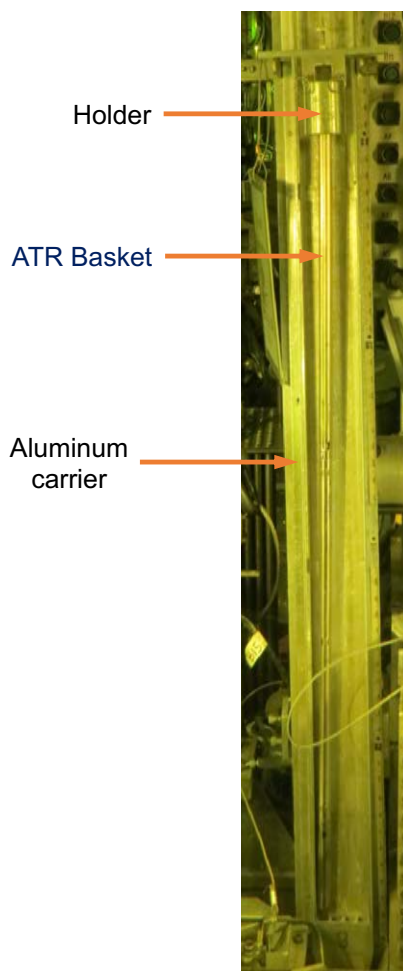


Figure 4. Neutron radiography setup for the LANL-MOD1A ATR Basket

^a Half-lives of In and Dy are 54 and 139.8 minutes, respectively.

3.2 Fluence wire examinations

Six neutron fluence wires were fabricated at PNNL, and two types of fluence wires (i) an iron-titanium-niobium and (ii) aluminum-cobalt alloys were used. The wire dimensions were typically 0.508 and 1.016 mm in diameter and height, respectively. Mass of each wire was measured as well. Fluence wires were encapsulated in electron beam sealed vanadium capsules with diameter of 1.27 mm and height of 8.64. The Co-Al wires were encapsulated separately from the other three wires. The vanadium tubes had identification codes stamped on the bottom. Details of the fluence wire fabrication were documented in a PNNL report [17]. Following irradiation in ATR, the fluence wires were returned to PNNL for analysis.

Each wire was cleaned prior to visual examination under a microscope to confirm the capsule identification. The individual wires were removed from the capsules. The niobium wires were dissolved in a mixture of nitric and hydrofluoric acid and a small aliquot was deposited on filter paper. For the gamma counting using low energy germanium (LEGe) detectors with thin beryllium windows were used to measure the 16.6 and 18.6 keV x-rays from the decay of niobium (^{93m}Nb) isotope with a half-life of 16.1 years. The gamma detectors were calibrated using National Institute of Standard and Technology (NIST) traceable standards. The performance of the gamma detectors is checked daily using control standards to confirm the energy, resolution, and efficiency calibrations and the energy. The activity of ^{94}Nb provided an internal radioactive tracer for the chemical separations. The ^{93m}Nb measurements followed the ASTM procedure E1297 [18].

3.3 Melt wire examinations

Melt wires are a form of passive instrumentation used to determine peak temperatures reached during irradiation testing. Nominal dimensions of melt wires are 0.5 mm and 2 mm in diameter and length, respectively. Melt wires were made of pure or alloy metals with a known composition and melting temperature and are encapsulated in inert gas within a sealed quartz capsule. Each individually encapsulated wire was selected as the best candidate to be placed in localized areas of interest within the internals of the experiment during irradiation. Specifically, two melt wires were placed inside holes within the TZM ring of each LANL capsule specifically designed for them. After irradiation, these melt wire capsules were then removed and visually inspected using a microscope to identify melting characteristics at AL. If the melt wire showed signs of melting, this indicates the peak temperature at that location exceeded the melting temperature of the melt wire, and alternatively if the melt wires did not melt, the melting temperature of the wires was not reached. Melting can manifest differently in various materials. Different characteristics seen during melting could include any combination of rounded edges where sharp features were previously present, formation of a spheroid within part or all of the wire, pooling at the low end of the capsule, buckling, or the development of bubbles or beads while the bulk of the material appears unaffected. Therefore, prior to the experiment, each melt wire was individually examined to identify specific melting characteristics observed in prototype tests completed in a furnace prior to experiment assembly.

3.4 Optical Inspection of Samples

Optical inspections of specimens were performed using a Dino-Lite AM73915MZTL digital microscope. Optical images were collected from front, back, and side of each YH_x disks. The microscope was calibrated using a NIST-certified external standard supplied by Klarmann Rulings, Inc (see Figure 5) with an uncertainty of ± 0.0007 mm.

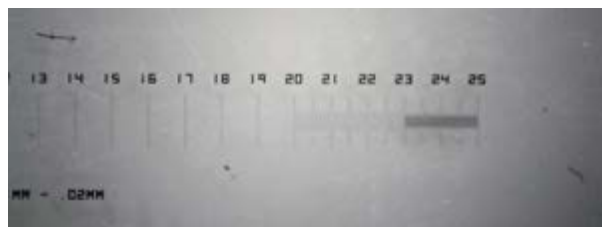


Figure 5. Stage Micrometer KR-812 as imaged on Dino-Lite AM73915MZTL digital microscope.

3.5 Mass, volume, and density measurements

A Mettler-Toledo XPR204 four-place analytical balance^b was used for mass measurements. The balance was calibrated by the INL Calibrations and Standards Laboratory. Prior to measurements and anytime a change in ambient temperature greater than 1°C was detected by the balance an automated internal adjustment was performed using calibration weights. The balance performance was checked daily before and after measurements with six external calibrated mass standards^c. The results from the external calibration check weights were recorded to evaluate for long term bias. For each sample an aluminum weigh pan was tared prior to sample measurement.

Volume measurements were made using a Micromeritics AccuPyc II 1345 Gas Displacement Pycnometer (see Figure 6). This instrument works by expanding helium gas between reference and sample chambers while measuring pressure and temperature change. It was assumed that the volume of the sample and reference chambers remain constant throughout the expansions. The instrument utilizes cups and inserts to hold the calibration standard or sample. The pycnometer was calibrated using a certified volume standard.



Figure 6. Micromeritics AccuPyc II 1345 gas displacement pycnometer

A 10 mL sample cup with a 1 mL insert was used in the control module to measure the volume of the large YH_x disks. A 1 mL cup was used for the calibration of the small volume module and a 0.1 mL cup/insert was used to measure the smaller YH_x DSC disks. A custom cup/insert was fabricated at the INL's mock-up shop with a 60% smaller volume than the 0.1 mL cup/insert supplied by the manufacturer to improve the accuracy. The uncertainty in the volume measurement was empirically determined by the manufacturer using Equation 1.

^b Identification number of the balance is 346089

^c Nominal masses of the standards are 1, 10, 20, 50, 100, and 200 g with identification numbers of 737544, 737364, 736181, 737433, 737787, and 737455, respectively

$$\Delta = 0.0003 (V_{\text{Chamber}} + V_{\text{Chamber+Specimen}}) \quad \text{Eq. 1}$$

where Δ is the uncertainty with 2-sigma (95.4%), and V is the volume of chamber with and without specimen.

The density of the material was calculated using Equation 2, where ρ is density, m is the mass, and V_s is the specimen volume. Average values were used for mass and volume when available. The uncertainty from mass and volume were propagated in GUM Workbench Pro v 2.4.1.406 to determine the total expanded uncertainty in the density value.

$$\rho = \frac{m}{V_s} \quad \text{Eq. 2}$$

3.6 Thermal diffusivity

The thermal diffusivity of fresh irradiated specimens was measured using laser flash analysis (LFA) in the Fresh Fuels Glove Box of AL. This glove box had an argon gas environment with 1 ppm oxygen (O_2) and < 5 ppm water (H_2O). A Netzsch LFA instrument was used by following ASTM standard E1461-13 [19]. Two different standard materials (Pyroceram 9600 (made of magnesium aluminosilicate glass) and >99.9% pure iron discs) were used to verify the calibration of the instrument and its detectors. A pilot laser was used to assure that no pulsed laser light would leak through to the temperature detector above specimens. To minimize any potential interaction of hydride specimens with their surroundings, specimen holders were painted with yttria paint (see Figure 7 for the LFA test setup). To increase the signal-to-noise ratio, an annular cap was placed directly on top of the sample. Ultra-high purity argon was used as the cover gas, which flowed through the sample chamber for 20 minutes before shutting the chamber inlet and outlet.

For all samples, LFA measurements were taken at 25 °C, 50 °C and 50 °C increments thereafter. The maximum measurement temperature was 800°C for fresh YH_x specimens while irradiated specimens were heated up to 850 or 1000°C for LFA measurements. The thermal diffusivity was obtained using the pulse-corrected Cowan model integrated into the Netzsch Proteus LFA analysis software, version 7.2 [20].

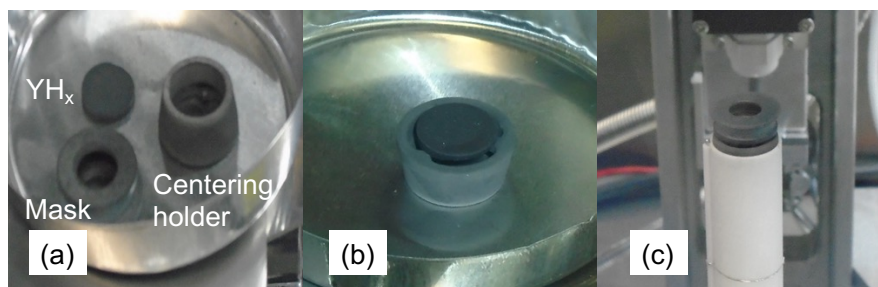


Figure 7. (a), Yttrium sample, centering cone holder, and mask (b) The yttrium hydride disc placed on the holder, (c) LFA test set-up with sample loaded.

4. STATUS OF THE YH_x PIE

Status of the PIE for FY22 is as follows. The retrieval of the ATR basket, neutron radiography, disassembly of fixtures, sample retrieval, and packaging with proper numbering were completed at HFEF. Issues due to specimen embrittlement were recorded during specimen retrieval process. The fluence wires were retrieved, packaged, and shipped to PNNL for gamma analysis. SiC passive thermometry specimens were shipped to ATR for acid cleaning prior to analysis. Melt wires were transferred to AL for

optical examinations. Due to dose limitations of the AL, YH_x specimens were shipped in groups for further PIE examinations. Transfer and examination of RUS specimens were delayed to next FY due to high dose rates. Optical and dimensional examinations, basic physical property measurements, and thermal property assessment of YH_x specimens commenced.

5. PIE RESULTS

5.1 Neutron radiography

Figure 8 shows the neutron radiographs of the ATR fixture at orientations of 0, 60, and 120° where six LANL capsules contained specimens from top to bottom. The color map from dark to white depicts zero to full neutron absorption contrast. Individual YH_x samples are visible with lighter contrast (tones close to white). Other components showed gray contrast where neutron absorption was lower than that for YH_x specimens. No defects or failures on the ATR basket and TZM capsules were detected after irradiation and following transportation from ATR to NRAD; all capsules and samples appeared to be intact.

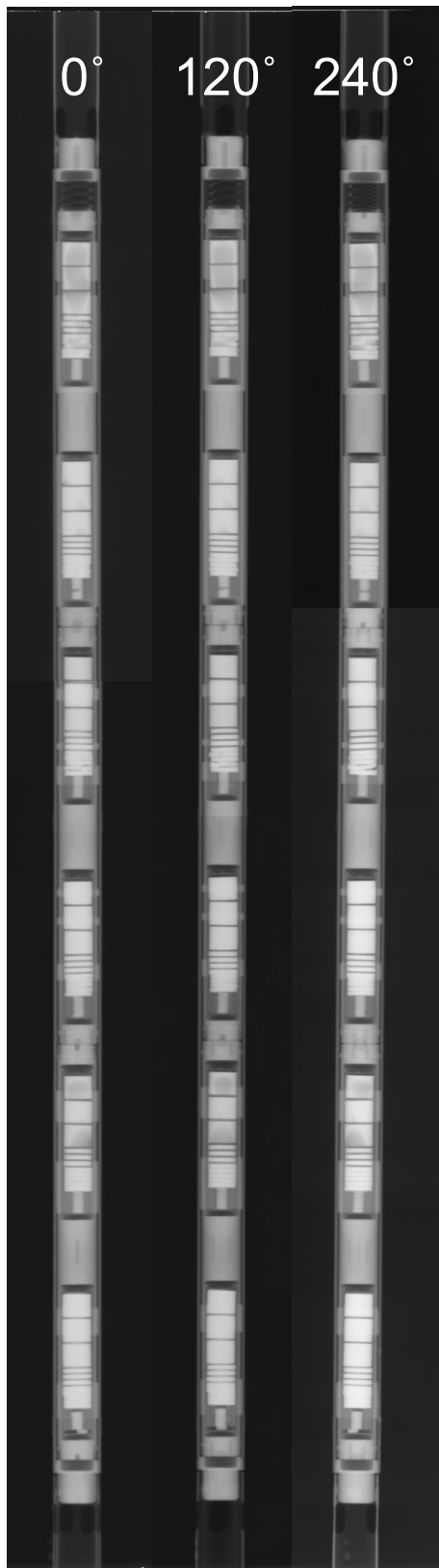


Figure 8. Neutron radiography of the ATR fixture and LANL capsule and YH_x specimens at angles of 0, 120, and 240°

Figure 9 provides a detailed view of neutron radiographs for capsules 1 to 6. Some regions of YH_x sample showed contrast variations where less neutron absorption was present (darker shade), such as Capsules 1, 2B, and 4. The contrast variations were more prominent in Capsules 1 and 2B.

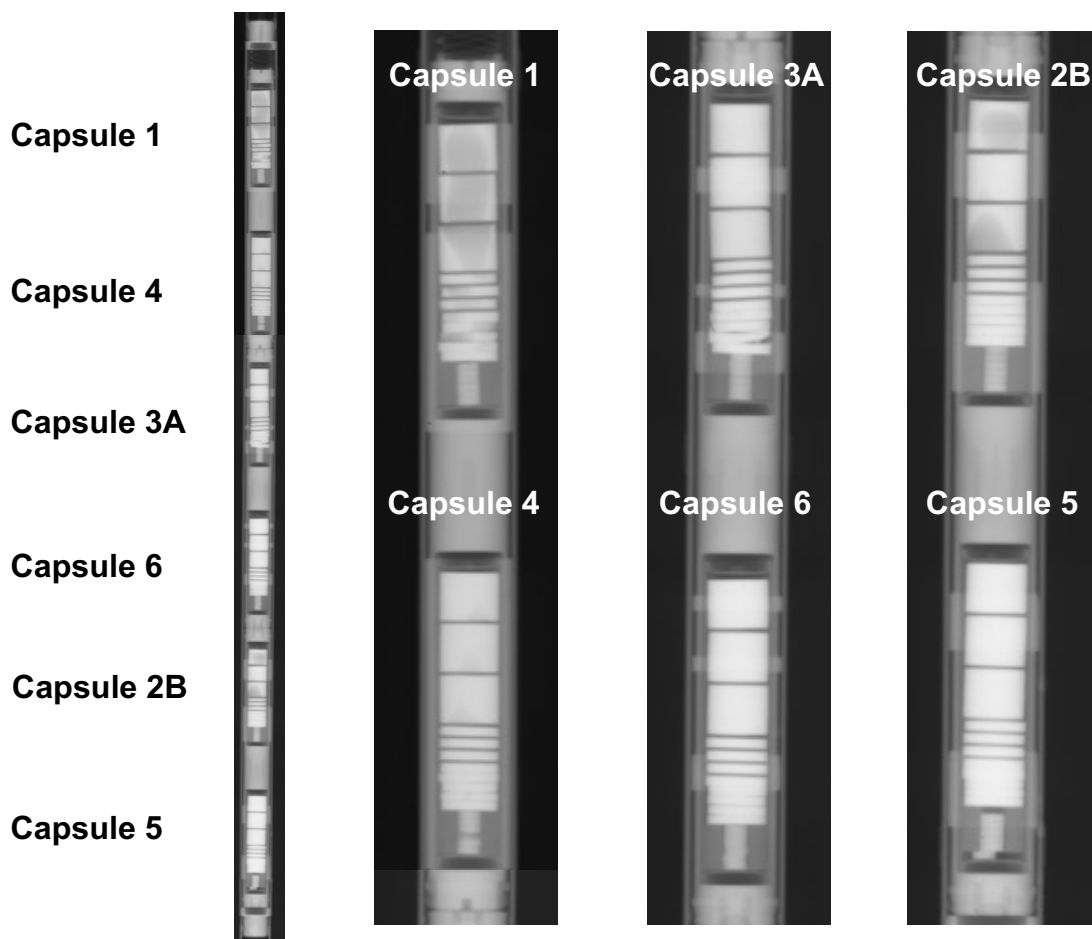


Figure 9. Neutron radiographs of individual capsules at angle of 240°

5.2 Specimen retrieval and transfer

After neutron radiography, the irradiation basket was disassembled in HFEE to access each capsule. Each LANL capsule then had both ends cut/removed using a slow speed saw as shown in Figure 10a. The samples were then gently pushed out of the open cylinder to access one YH_x sample at a time. TZM capsules exhibited brittle behavior during capsule opening. During the cutting of the LANL capsule with the low-speed saw, a crack initiated and propagated through the cylinder (see Figure 10b). As a result, the TZM capsule fragmented into two or more pieces, as shown in Figure 10c. This behavior was observed for all TZM capsules. Due to the brittleness of YH_x , some specimens were acquired as powdered or broken conditions during remote handling in the hotcell, as shown in Figure 11.

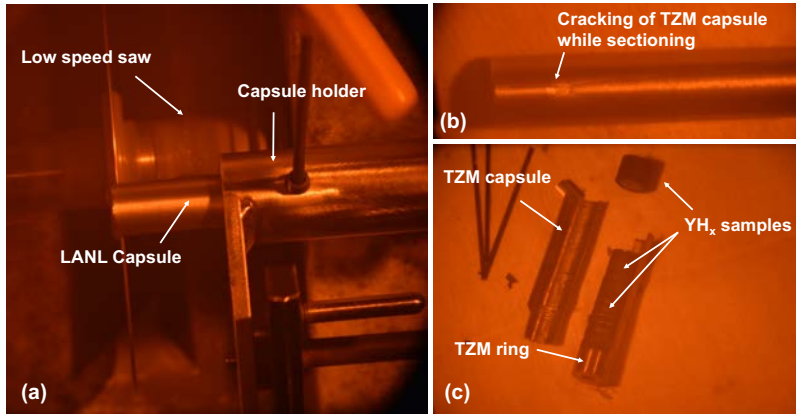


Figure 10. (a) LANL capsule sectioning (b) cracking of LANL capsule, and (c) sectioned capsule with specimens

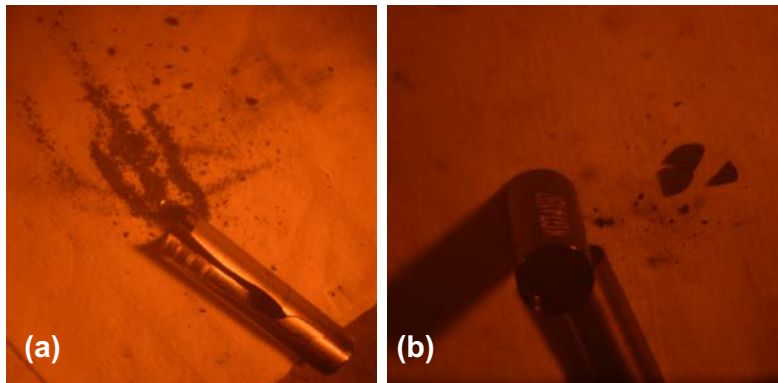


Figure 11. (a) Powdered and (b) ruptured specimens

Table 2 shows the status of the samples after capsule opening using remote manipulators at HFEF. Several of the samples failed prior to handling with manipulators thus exhibiting their extreme brittleness. The number of broken, powdered, and bonded specimens were 3, 5, and 6 respectively. For capsule 3A, bonded specimens were all DSC type, no TZM sheet was present in between. DSC1, 2, and 3 were bonded together to form a single specimen, while DSC 4 and 5 bonded to form another. In total, 88 of 102 YH_x specimens were retrieved as intact condition.

Table 2. Status of the specimen after capsule opening

Specimen name	Capsule identifications					
	600-1	700-2B	800-3A	600-4	700-5	800-6
RUS1	Intact	Intact	Intact	Intact	Intact	Intact
RUS2	Intact	Intact	Intact	Intact	Intact	Intact
RUS3	Intact	Intact	Intact	Intact	Intact	Intact
GDOES1	Intact	Intact	Intact	Powdered	Intact	Intact
GDOES2	Intact	Intact	Intact	Powdered	Intact	Intact
GDOES3	Intact	Intact	Intact	Powdered	Bonded to TZM	Intact
GDOES4	Intact	Intact	Intact	Powdered	Intact	Intact
GDOES5	Intact	Intact	Broken	Powdered	Intact	Intact
TEM1	Intact	Intact	Intact	Intact	Intact	Intact
LFA1	Intact	Intact	Broken	Intact	Intact	Intact
LFA2	Intact	Intact	Intact	Intact	Intact	Intact
DSC1	Intact	Intact	Bonded together	Intact	Intact	Intact
DSC2	Intact	Intact		Intact	Intact	Intact
DSC3	Intact	Intact	Bonded together	Intact	Intact	Intact
DSC4	Intact	Intact		Intact	Intact	Intact
DSC5	Intact	Intact		Intact	Broken	Intact
DSC6	Intact	Intact	Intact	Intact	Intact	Intact

All retrieved specimens, including YH_x, TZM sheets and rings, melt wires, SiC thermometry stick, and fluence wires, were placed into individual aluminum containers having specific serial numbers. Fluence wires were transferred to PNNL for gamma analysis to determine the neutron fluence, and SiC thermometry were transferred to ATR facility for cleaning and subsequent temperature analysis. Melt wires were transferred to AL to conduct visual inspections to identify potential temperature range. YH_x specimens were transferred in groups due to the dose limitations. YH_x specimens, except the RUS specimens, were transferred during FY22.

5.3 Fluence wires

Detailed analysis of the fluence wires has been provided by PNNL and included in the PIE documentation. Figure 12 shows the fluence wire results along the ATR reactor elevation at the B2 irradiation position, based on activity measurements. The fast fluence for neutron energies greater than 0.18 MeV was measured as 1.17, 1.27, and 1.15 10^{21} n/cm². Measured values were consistent with the calculated neutron fluence values as shown in Table 3.

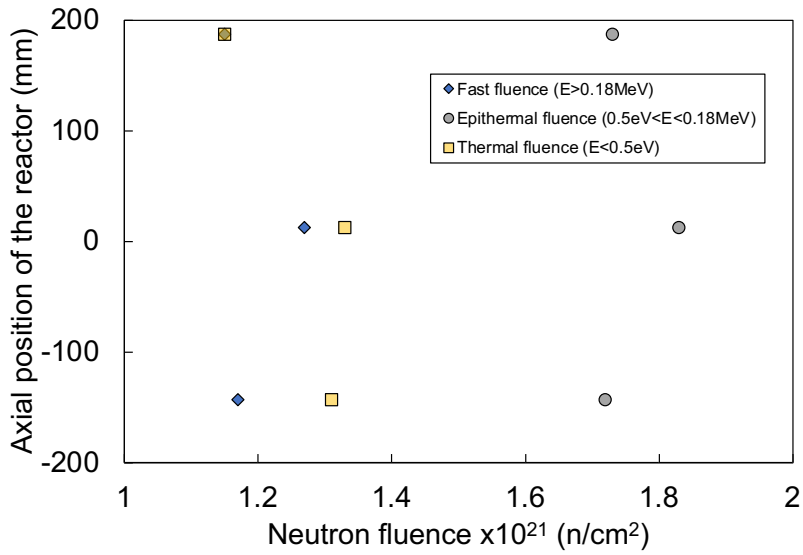


Figure 12. Axial profile of the neutron fluence based on fluence wire analysis

Table 3. Fluences levels on the fluence wires as calculated and measured

Capsule	Modeled fast (>0.1 MeV) fluence x10 ²¹ (n/cm ²)	Measured fast (>0.1 MeV) fluence x10 ²¹ (n/cm ²)
1 (600°C)	1.61	1.28
4 (600°C)		
3A (800°C)	1.71	1.40
6 (800°C)		
2B (700°C)	1.67	1.27
5 (700°C)		

5.4 Melt wires

Optical photographs of the melt wires after sample retrieval are shown in Figure 13, 14, and 15. Most of the melt wires were damaged during retrieval due to getting stuck within the TZM ring during irradiation. Therefore, limited information was obtained from the melt wire assessment (see Table 4).

The main takeaways from the melt wire analysis are as follows. The capsules that were expected to be at 600°C experienced a radial temperature gradient where one side was >630°C and other side was <577°C. Capsules that were expected to be around 800°C experienced higher temperatures, above 865°C. Temperatures were above 681 °C for the capsules expected to be 700°C , but no maximum temperature was determined due to lack of melt wires operating above 700°C.

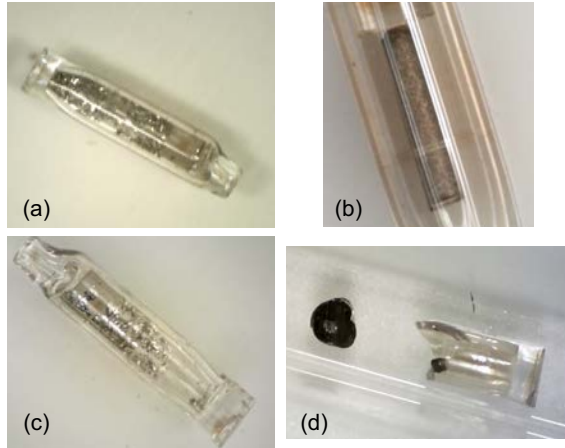


Figure 13. Photographs of melt wires from capsules 1 (a and b) and 4 (c and d)

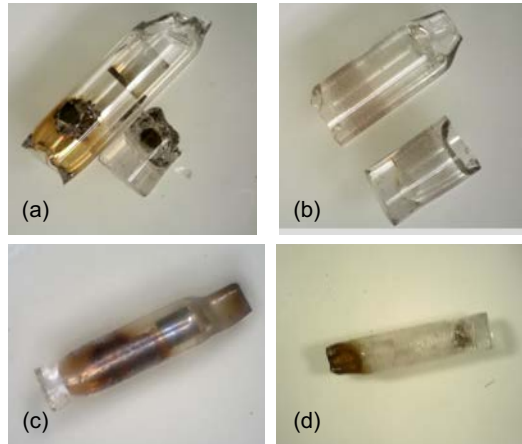


Figure 14. Photographs of melt wires from capsules 2B (a and b) and 5 (c and d)

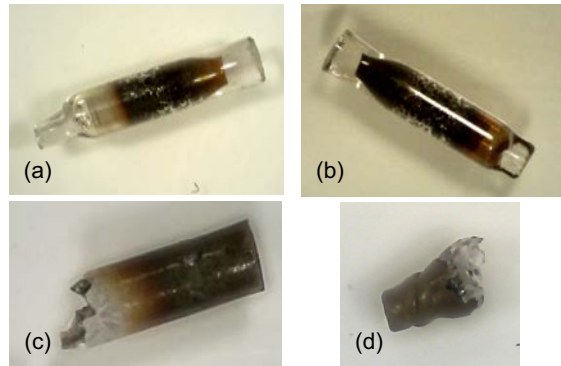


Figure 15. Photographs of melt wires from capsules 3A (a and b) and 6 (c and d)

Table 4. Melt wire examination results

Capsule	Irradiation temperature (°C)	Melting point (°C)	Melt wire	Quartz capsule condition	Qualitative results
1	609	577	88Al 12Si	Intact	No Melting
1	609	630	100Sb	Intact	Melted
4	610	630	100Sb	Intact	Melted
4	610	577	88Al 12Si	Broken	Undetermined
3A	811	865	1.8Be 98.2Cu	Damaged	Likely Melted
3A	811	865	1.8Be 98.2Cu	Damaged	Likely Melted
6	813	865	1.8Be 98.2Cu	Broken	Undetermined
6	813	865	1.8Be 98.2Cu	Broken	Undetermined
2B	769	660	100Al	Broken	Melted
2B	769	681	49Au 16Cu 23Zn 7.5Mn 4.5Ni	Broken	Undetermined
5	715	681	49Au 16Cu 23Zn 7.5Mn 4.5Ni	Intact	Melted
5	715	660	100Al	Intact	Melted

5.5 Optical inspection of YH_x specimens

Optical photographs of irradiated YH_x specimens are shown in Table 5 to 10. Each table includes front, back, and side views of samples where available. Pictures of powder metallurgy fabricated samples after irradiation are in Table 5, 7, and 9. Massively hydrided specimens after irradiation are shown in Table 6, 8, and 10. Significant alterations to the physical appearance of the irradiated YH_x was observed in large diameter specimens (GDOES, TEM, and LFA) of capsule #1 (see Table 5) relative to the expected color of a fresh specimen (light or dark-blueish). Optical photographs of GDOES2 and TEM1 indicated a significant localized modification of the specimens that penetrated through the thickness of the specimens. A similar attack was present for LFA1 and LFA2 specimens, but it was not as significant as in other two. By examining the back surface of LFA2 specimen, discoloration was observed where the YH_x and TZM ring were in contact. However, this interaction was limited to surface of the YH_x. Not all YH_x samples in contact with TZM experienced such an interaction. For small specimens (DSC), no significant YH_x/TZM interaction was determined although these specimens were sleeved with TZM ring.

Optical inspections of capsule #4 specimens (Table 6) indicated limited TZM/YH_x interaction, as compared to capsule #1 although expected irradiation temperatures were similar. Furthermore, limited TZM/YH_x interactions were identified for the rest of YH_x specimens in other capsules. Based on these observations, the significant discoloration of capsule #1 specimens, excluding DSC specimens, could not be explained by the chemical attack of TZM since the driving force for the chemical interaction (e.g., temperature) was higher for other capsules where no significant interaction was determined. Therefore, it was speculated that this behavior might originate from the hydride fabrication process. Dimensions of intact samples were also measured, and data were included in the PIE documentation.

Table 5. Optical pictures of powder metallurgy manufactured YH_x , irradiated at 600°C

Capsule #1	Front	Back	Side
GDOES1			
GDOES2			
GDOES3			
GDOES4			
GDOES5			
TEM1			
LFA1			
LFA2			
DSC1			
DSC2			
DSC3			
DSC4			
DSC5			
DSC6			

Table 6. Optical pictures of massively hydrided YH_x , irradiated at 600°C

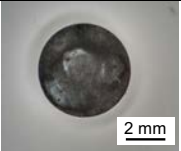
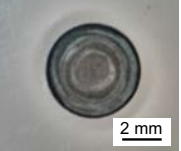
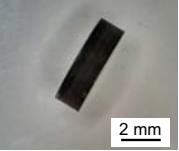
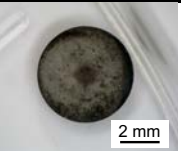
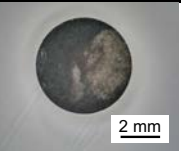
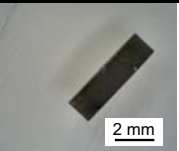
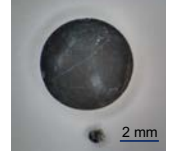
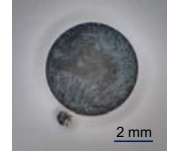
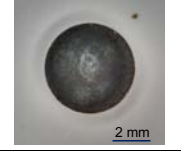
Capsule #4	Front	Back	Side
GDOES1	Pictures are not available due to powdering		
GDOES2	Pictures are not available due to powdering		
GDOES3	Pictures are not available due to powdering		
GDOES4	Pictures are not available due to powdering		
GDOES5	Pictures are not available due to powdering		
TEM1			
LFA1			
LFA2			
DSC1			
DSC2			
DSC3			
DSC4			
DSC5			
DSC6			

Table 7. Optical pictures of powder metallurgy manufactured YH_x , irradiated at 700°C

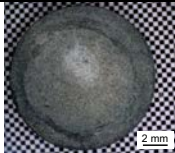
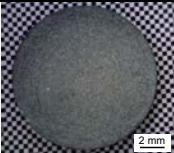
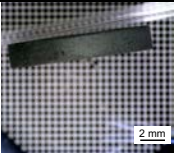
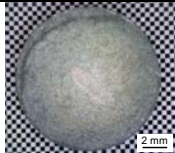
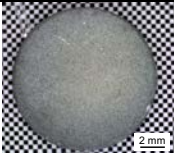
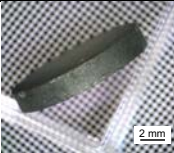
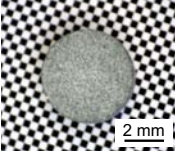
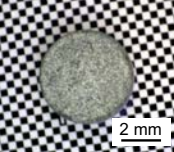
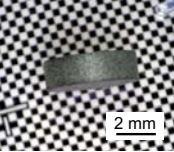
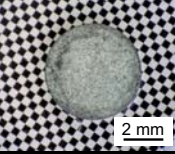
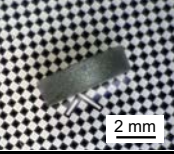
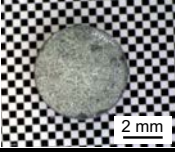
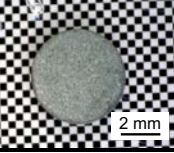
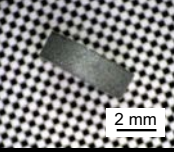
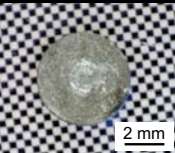
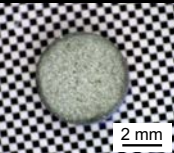
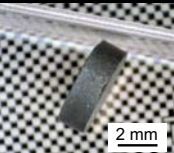
700-2B	Front	Back	Side
GDOES1			
GDOES2			
GDOES3			
GDOES4			
GDOES5			
TEM1			
LFA1			
LFA2			
DSC1			
DSC2			
DSC3			
DSC4			
DSC5			
DSC6			

Table 8. Optical pictures of massively hydrided YH_x , irradiated at 700°C

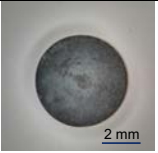
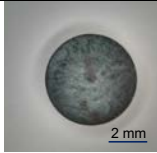
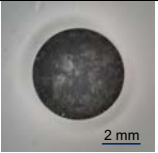
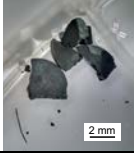
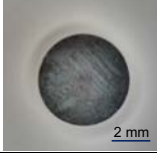
Capsule #5	Front	Back	Side
GDOES1			
GDOES2	Pictures are not available due to powdering		
GDOES3			
GDOES4			
GDOES5	Pictures are not available due to powdering		
TEM1			
LFA1			
LFA2			
DSC1			
DSC2			
DSC3			
DSC4			
DSC5			
DSC6			

Table 9. Optical pictures of powder metallurgy manufactured YH_x , irradiated at 800°C

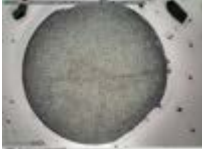
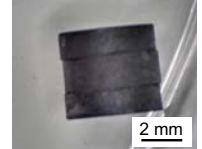
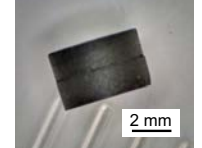
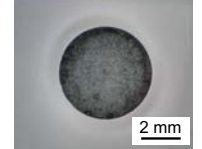
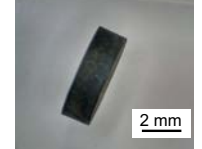
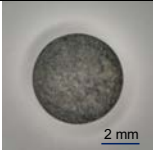
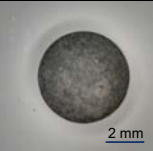
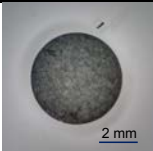
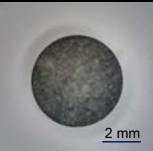
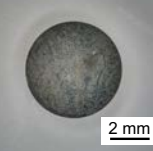
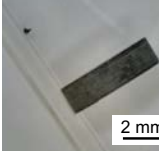
Capsule 3A	Front	Back	Side
GDOES1			
GDOES2			
GDOES3			
GDOES4			
GDOES5			
TEM1			
LFA1			
LFA2			
DSC1 DSC2 DSC3	 2 mm	 2 mm	 2 mm
DSC4 DSC5	 2 mm	 2 mm	 2 mm
DSC6	 2 mm	 2 mm	 2 mm

Table 10. Optical pictures of massively hydrided YH_x, irradiated at 800°C

800-6	Front	Back	Side
GDOES1			
GDOES2			
GDOES3			
GDOES4			
GDOES5			
TEM1			
LFA1			
LFA2			
DSC1			
DSC2			
DSC3			
DSC4			
DSC5			
DSC6			

5.6 Mass, volume, and density measurements of YH_x

Mass, volume, and density of 31 YH_x specimens were completed from each capsule, and these measurements were recorded for each specimen. Post-irradiation measurements were compared with those for pre-irradiation values as provided by LANL. Noting that, the manufacturing pedigree was limited, and uncertainties related to fresh specimen measurements were largely absent. Fresh specimen mass measurements included having 4-digit sensitivity (mostly 2-digit sensitivity after the point). Specimen volumes were calculated using dimensional measurements as opposed to INL's gas pycnometry approach for irradiated samples.

Figure 16 shows the percent mass variation of YH_x specimens for each capsule after irradiation. No systematic trend was observed. YH_x specimens both gained and lost mass. If mass values were averaged over a single capsule, YH_x specimens in capsules 1, 3A, 2B, 5 showed mass gain, vice versa for capsules 4 and 6. Average percent mass variations were 0.49, -0.89, 0.66, -1.34, 0.08, 0.05 % for capsules 1, 4, 3A, 6, 2B, 5. Noticeably, mass variations were low for capsule that were irradiated at 715 and 769 °C. the latter was the capsule with a crack. Remaking that, outliers of the (maximum mass variations) were reached to ± 8 %. Some mass variation was due to the material loss during specimen transfer and

handling, owing to the brittleness of hydrides. Mass gain could have occurred from oxidation of the fabricated samples between their initial mass measurement and loading in the LANL capsule, and interactions between the YH_x and the TZM.

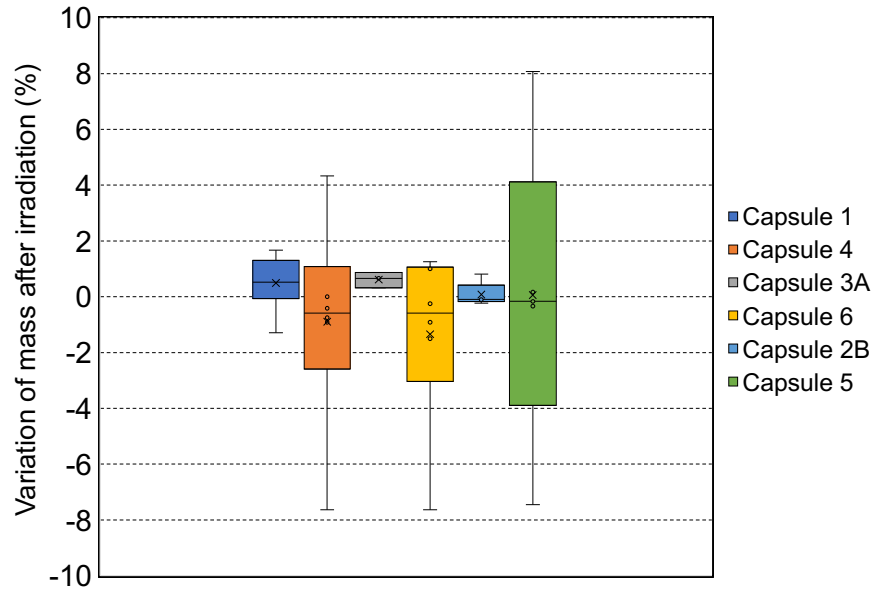


Figure 16. Percent variation of specimen masses after irradiation

Figure 17 shows the percent variation of YH_x specimens' volume from each LANL capsule after the irradiation. On the average, volume of YH_x specimens were reduced as compared to initial values. Similar to mass variations, loss of materials during specimen transfer and handling were mainly responsible for the volume reduction.

On the other hand, Figure 18 identifies a density increase in YH_x specimens, independent of any material loss as stated for mass and volume measurements. TZM and YH_x interaction, and oxidation could cause mass gain and consequent density increase in some YH_x specimens, but density increase was consistent with the majority of specimens. Thus, the density increase was speculated due to potential hydrogen loss where hydrogen content measurement required. For powder metallurgy specimens, densification process (e.g., closure of pores) was also considered as an additional parameter.

Mass, volume, and density measurements are still ongoing. With more data and completion of additional PIE, a better explanation to this data is to be provided.

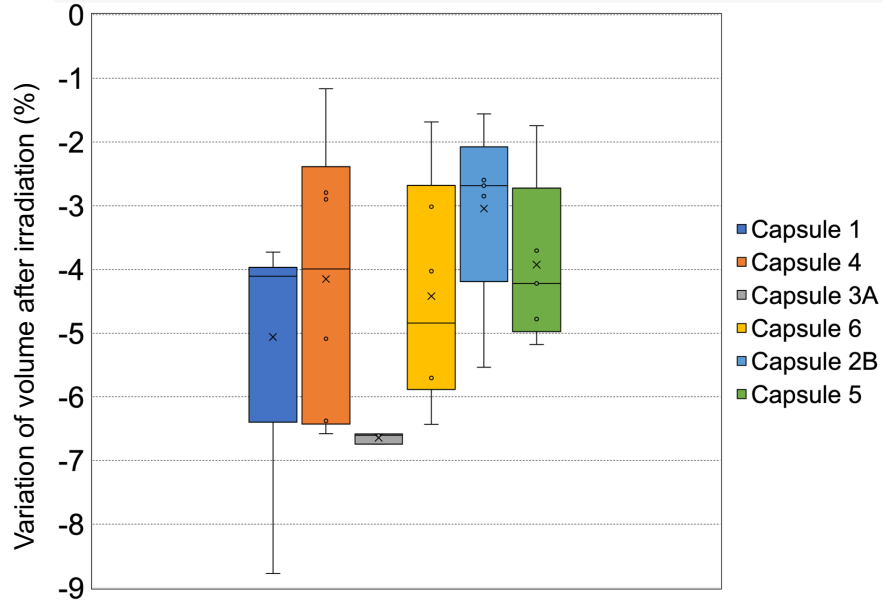


Figure 17. Percent variation of specimen volumes after irradiation

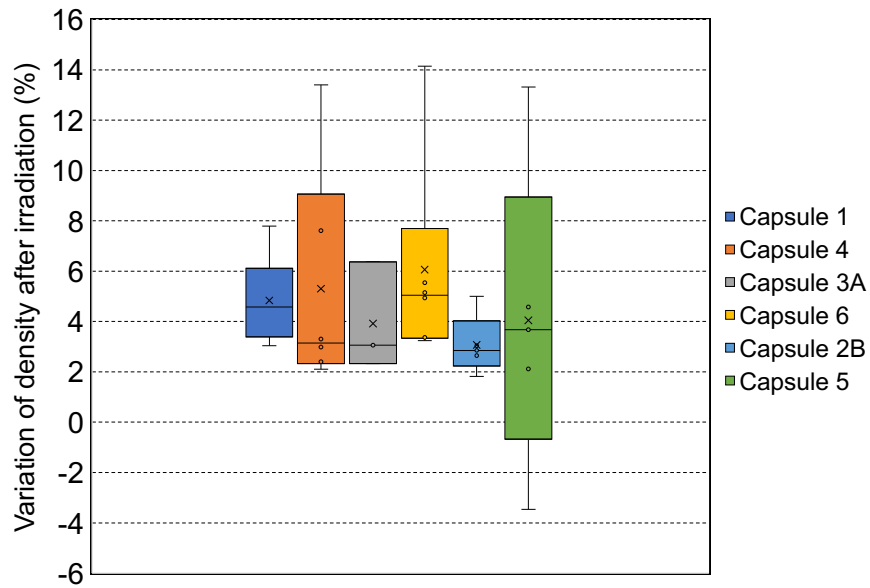


Figure 18. Percent variation of specimen density after irradiation

5.7 Thermal diffusivity results

The thermal diffusivity (mm^2/s) values of fresh and irradiated yttrium hydride discs are shown in Figure 19. The thermal diffusivity of all specimens reduced as temperature increased, similar to ceramics' thermal diffusivity behavior. The thermal diffusivity of the fresh sample showed no significant difference for heating and cooling stages, indicating no or negligible hydrogen loss. The thermal diffusivity was $52 \text{ mm}^2/\text{s}$ at room temperature, and it decreased to $8 \text{ mm}^2/\text{s}$ at $800 \text{ }^\circ\text{C}$.

The thermal diffusivity values for the irradiated specimens were approximately 30% lower than the fresh yttrium hydride throughout the measured temperature range. Noting that, these LFA specimens originated from the cracked capsule 2B where the sample atmosphere may have deviated from its design. The irradiated specimen that was heated to 850°C showed no substantial difference in the diffusivity values for heating and cooling stages. On the other hand, the diffusivity values of the irradiated specimen, heated to 1000°C, showed some degradation upon cooling below 400 °C. This behavior was explained as follows. Above 400°C, the diffusivity values from heating and cooling stages were similar since YH_x was present as a single phase. With cooling (below 400°C), the potential hydrogen loss caused a shift in the stoichiometry where yttrium was able to precipitate.

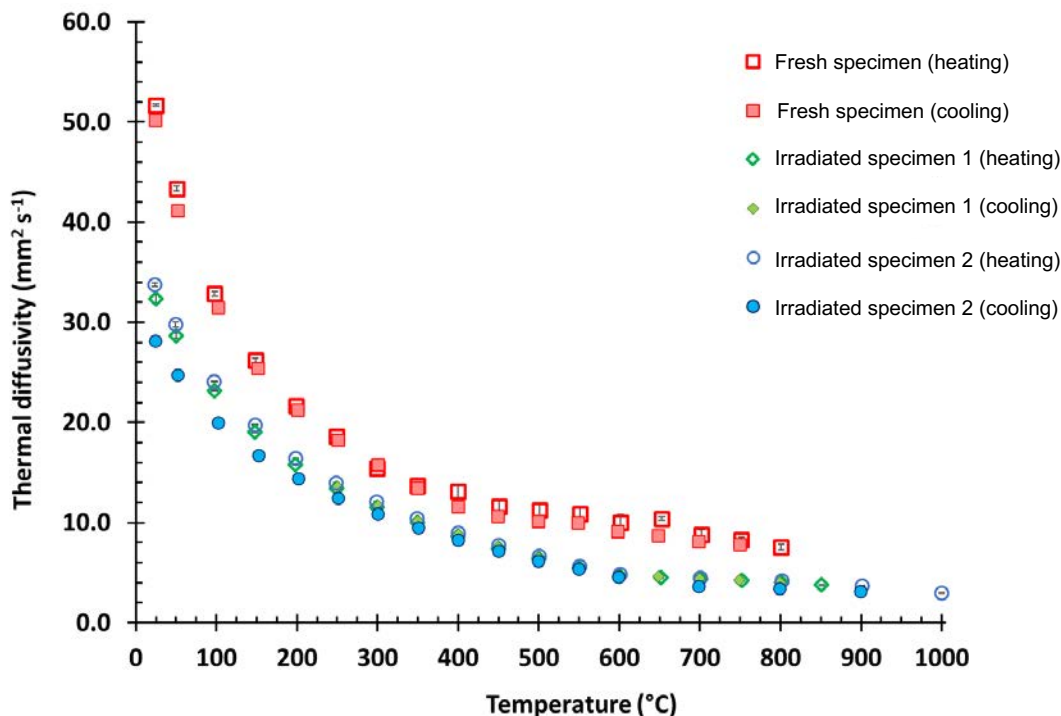


Figure 19. Mean thermal diffusivity ($\text{mm}^2 \text{s}^{-1}$) as a function of temperature for a fresh yttrium hydride disc as well as two irradiated yttrium hydride discs from capsule #2B ($T_{\text{irr}}=700^\circ\text{C}$).

6. DEVELOPMENT HYDROGEN MEASUREMENT TECHNIQUE BY INERT GAS FUSION (IGF)

Hydrogen content measurements are essential to assess potential hydrogen evolution from the YH_x moderator resultant from neutron irradiation. However, reliable analytical techniques, except for hot vacuum extraction, which is not currently available at INL PIE facilities, is lacking for materials containing hydrogen at very high concentrations (>1000 wt. ppm) due to the limitations of analytical instruments. INL possesses an inert gas fusion (IGF) analyzer to determine hydrogen contents in irradiated materials. A typical IGF instrument can measure hydrogen contents below 500 wt. ppm using standards without detector saturation, however solid yttrium hydride with 1.89 stoichiometry ratio ($YH_{1.89}$) contains ~ 21000 wt. ppm of hydrogen that is well beyond reliable measurement limits of IGF analyzer. Therefore, current IGF instruments cannot measure hydrogen in the metal hydride.

To overcome this problem, an alternative analytical method was developed where the IGF analyzer could be used. The method is based on diluting hydrogen content down to instrument measurable levels by mixing YH_x with an inert material (yttria powder). Prior to the dilution process, yttria was subjected to

baking treatment in argon environment to remove any residual hydrogen or moisture. Blank measurements are performed on the yttria diluent powders to ensure that they do not contribute any hydrogen to the measurement. The diluted YH-yttria powders are measured and all measured hydrogen is attributed to the YH powders. Therefore, the hydrogen content of initial YH_x specimens can be determined.

For the method development, a fresh bulk YH_x specimen (4.8069 g) with $x = 1.89-1.91$ (LANL-provided) was used. The initial hydrogen content of the YH_x was determined by mass balance measurements. The estimated hydrogen content of the specimen was in the range of 21000-21100 wt. ppm. YH_x specimens were also prepared using mortar and pestle. Then, YH_x particles were sieved to certain size (40-60 μm). It was assumed that hydrogen loss from this process was negligible due to the high stability of YH_x at ambient temperature. After powder preparation, it was mixed with ~ 10 μm yttria powder to a 1:100 mass ratio in an Ar atmosphere. The resultant mixture was mixed using a vortex mixer for 10 minutes to increase homogeneity. Once mixed, 90-100 mg portions from the mixture were divided into tin capsules for the inert fusion analysis (see Figure 20 for the mixture preparation process). This process decreased the hydrogen content of the YH_x/yttria mixture to IGF measurable levels where hydride standards were commercially available.

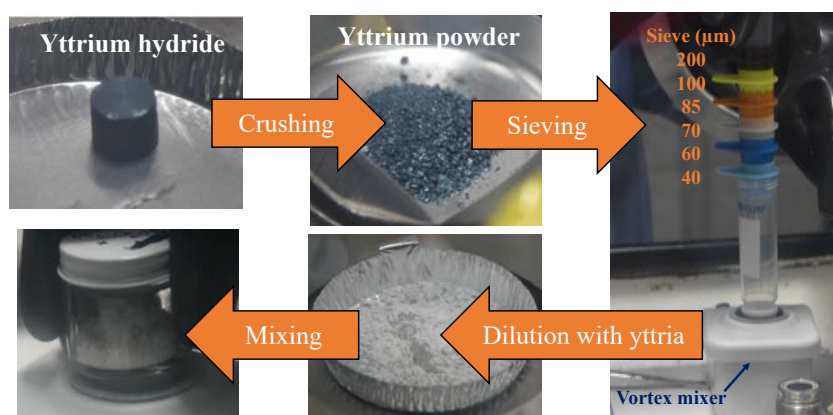


Figure 20. Process of YH_x dilution process for IGF analysis

Prepared YH_x/yttria mixtures were put inside heat-sealed plastic bags in an argon environment and transferred to another argon glove box where the IGF analyzer was located. For IGF analysis, an ELTRA ONH-2000 inert fusion combustion analyzer was used. Prior to specimen measurements, certified reference titanium hydride (TiH₂) materials were analyzed for calibrations and to check the instruments performance in the calibration range. In total, 8 YH_x/yttria mixtures and 11 yttria specimens were analyzed using IGF analyzer. Intermediate certified check specimen runs were performed to ensure instrument accuracy. A single mixture specimen test includes YH_x powder, yttria powder, and tin sample holder. Yttria and sample holder potentially contain hydrogen, they were also separately analyzed multiple times. The average hydrogen content of yttria powder and sample holder material were accepted as a representative hydrogen content for those. Thus, the hydrogen content of a single mixture specimen was subtracted from average hydrogen contents of yttria and sample holder to determine the hydrogen content of YH_x powder only, as shown in Equation 3.

$$M_{hydride}^H \approx M_{mixture}^H - M_{dilutant}^H + M_{holder}^H \quad \text{Eq. 3}$$

where M represents the mass, subscripts indicate hydride (YH_x), mixture, dilutant, and holder. The exponent is for hydrogen.

Table 11 shows the mass and IGF- measured hydrogen contents of yttria powder samples (yttria and sample holder). In total, 11 samples were tested, and the average hydrogen content was determined as 42

wt. ppm. Because, specimens were inserted into the holders, no separate holder measurements were performed. The maximum and minimum values were 51 and 37 wt. ppm, respectively. The average value was used for the dilution and sample holder corrections.

Table 11. Hydrogen content of yttria powder specimens as measured by IGF

#	Mass (g)	Hydrogen content (wt. ppm)
1	0.0908	42
2	0.0943	51
3	0.0898	48
4	0.0980	40
5	0.0993	43
6	0.0500	42
7	0.0452	39
8	0.0492	37
9	0.0508	34
10	0.0463	44
11	0.0460	39
Average		42

Table 12 shows the mass measurement of yttria powder, YH_x powder, and their mixture. In total 8 mixture specimens were prepared to perform IGF for hydrogen content measurements.

Hydrogen measurement results of the prepared YH_x specimens are shown in Table 13, as well as the dilutant corrected and back calculated. The average hydrogen content of YH_x - yttria mixture were determined as 250 wt. ppm where maximum and minimum values were 263 and 239 wt. ppm, respectively. The effect of the dilutant and sample holder were subtracted from the mixture results as shown in the second column of Table 13. Final hydrogen content of the $YH_{1.189-1.191}$ specimen was back calculated. The back calculated hydrogen content results (20900 wt. ppm) were in good agreement with the expected hydrogen content of the specimen (21000 wt. ppm). The fresh specimen results showed that this method was applicable to the hydrogen content measurements of YH_x and will be adequate for assessing the hydrogen content for hydride moderators. As hydrogen content measurement are the single-most important piece of PIE data, additional confirmatory methods, such as vacuum hot extraction, should be pursued.

Table 12. Mass measurements of yttria, YH_x , and mixture specimens

Test #	Yttria (g)	YH_x (μ g)	Mixture (g)
1	0.0919	912	0.0928
2	0.0970	963	0.0980
3	0.0945	937	0.0954
4	0.0953	945	0.0962
5	0.0982	975	0.0992
6	0.0974	967	0.0984
7	0.0960	953	0.0970
8	0.0990	983	0.1000

Table 13. Hydrogen content measurements of mixture, YH_x , and back calculated bulk YH_x , and stoichiometry ratio (H:Y)

Test #	Mixture total (wt. ppm)	Dilutant corrected YH_x powder (wt. ppm)	Back calculated YH_x specimen (wt.ppm)
1	263	221	22200
2	261	219	22100
3	255	213	21400
4	252	210	21100
5	243	201	20200
6	239	197	19800
7	246	204	20500
8	240	198	19900
Average	250	208	20900

7. CONCLUSIONS AND FUTURE WORK

Status of the PIE activities for YH_x solid moderator and initial PIE results are reported. During this FY, non-destructive neutron radiography examination of samples was performed, and specimen transfers from HFEF were completed. 96 (out of 102) YH_x specimens were transferred to the PIE facility while the remaining samples will be transferred when dose rates allow. All passive instrumentation samples were also transferred or shipped to relevant facilities and laboratories. The main observations and conclusions from the initial phase of the PIE are:

- (i) Neutron radiography indicated that TZM capsules were mechanically intact, and all YH_x specimens kept their main geometrical shape, but some misalignments and bending were observed. Contrast in the radiographs was observed, indicating some hydrogen loss/redistribution in some YH_x specimens from capsules 1,4, and 2B. No specific cause has been identified at this time since there was no pattern for the hydrogen loss.
- (ii) Retrieval of melt wires was not completely successful as several of the melt wire quartz ampules ‘bonded’ to the TZM ring and could not be removed without damage. Therefore, limited information was obtained from melt wires. Wire examination of capsules 1 and 4 indicated a radial temperature-gradient at the axial location of melt wires. If this gradient was persistent in the specimen regions, it would impact the hydrogen redistribution. Assessment of wires also showed that temperature values were higher than the simulation results for capsules 3A and 6.
- (iii) Most of YH_x specimens showed good mechanical integrity during specimen retrieval process although the specimens are brittle. Only 14 (out of 102) specimens were in failed condition.
- (iv) Optical inspection of specimens from capsule 1 indicated that some samples underwent a significant reaction. These areas of significant reaction were observed optically and correlate with the contrast regions observed in neutron radiographs. This dramatic modification in the sample requires additional PIE techniques that were not previously planned to assess the sample state and composition in these regions. Many hypotheses abound about what may have occurred, but additional measurements are required to provide conclusions. Samples from other capsules did not show the same chemical interactions even at higher temperatures. During specimen transfers additional specimens were broken and granulated. Understanding neutron radiography and optical inspection data together, it was concluded that a detailed fabrication pedigree was needed to provide a complete explanation for these observations.
- (v) Mass, volume, and density measurements of specimens commenced. Initial data shows that some hydrogen loss might occur in all specimens, based on density variations. However, this data must be understood with potential mass losses during specimen handling, partial mass gain due to oxidation, potential chemical interactions between TZM and YH_x , and the lack of measurement and calculation uncertainties from sample fabrication.
- (vi) Thermal diffusivity measurements clearly showed that both fresh and irradiated YH_x had high thermal stability up to 800°C where thermal diffusivity was not affected by a heating-cooling cycle. Some thermal property degradation was determined below 400°C for the specimen that was heated to 1000°C. This degradation was not present at elevated temperatures.

The irradiated YH_x PIE activities are still ongoing, and understanding of the data will augment with additional PIE data. For FY23, YH_x and TZM examinations will be completed. Some PIE activities will be modified based on the sample conditions and initial PIE results reported here. Optical inspections showed that assessment of hydrogen distribution and content in irradiated specimens are crucial for the hydride moderator development. Therefore, high resolution neutron tomography will be performed on selected specimens. Furthermore, more metallographic characterizations will be performed on specimens to understand TZM - YH_x interactions.

Page intentionally left blank

8. REFERENCES

- [1] A microreactor program plan for the Department of Energy INL/EXT-20-58191, Idaho National Laboratory, Idaho Falls, 2020, p. 23.
- [2] W.M. Mueller, Chapter 2 - Hydrides in Nuclear Reactor Applications, in: W.M. Mueller, J.P. Blackledge, G.G. Libowitz (Eds.), *Metal Hydrides*, Academic Press 1968, pp. 21-50.
- [3] J.B. Vetrano, Hydrides as neutron moderator and reflector materials, *Nuclear Engineering and Design* 14(3) (1971) 390-412.
- [4] J.C. Marshall, R. Van Houten, W.G. Baxter, Yttrium hydride moderator evaluation — in-pile thermal stability, United States, 1962.
- [5] R. Van Houten, Selected engineering and fabrication aspects of nuclear metal hydrides (Li, Ti, Zr, and Y), *Nuclear Engineering and Design* 31(3) (1974) 434-448.
- [6] J.P. Blackledge, Chapter 10 - Yttrium and Scandium Hydrides, in: W.M. Mueller, J.P. Blackledge, G.G. Libowitz (Eds.), *Metal Hydrides*, Academic Press 1968, pp. 441-489.
- [7] X. Hu, H. Wang, K. Linton, A. Le Coq, K. Terrani, *Handbook on the Material Properties of Yttrium Hydride for High Temperature Moderator Applications*, Oak Ridge National Lab. (ORNL), Oak Ridge, TN (United States), 2021, p. Medium: ED.
- [8] A.P. Shivprasad, T.E. Cutler, J.K. Jewell, V.K. Mehta, S.W. Paisner, C.A. Taylor, C.N. Taylor, H.R. Trellue, D.W. Wootan, E.P. Luther, *Advanced Moderator Material Handbook*, Los Alamos National Laboratory, United States, 2020, p. Medium: ED; Size: 66 p.
- [9] J.M. Fackelmann, J. Gedwill, M A, J. Krause, H H, *Survey of zirconium, yttrium, and cerium hydrides for reflector application in the GCRE*, ; Battelle Memorial Inst., Columbus, Ohio, 1960, p. Medium: ED; Size: Pages: 86.
- [10] E.S. Funston, *Physical properties of yttrium hydride A symposium on metallic moderators and cladding materials: Fall meeting of the metallurgical society*, Metallurgical Society, American Institute of Mining, Metallurgical and Petroleum Engineers, Philadelphia, 1960.
- [11] M. Ito, J. Matsunaga, D. Setoyama, H. Muta, K. Kurosaki, M. Uno, S. Yamanaka, Thermal properties of yttrium hydride, *Journal of Nuclear Materials* 344(1) (2005) 295-297.
- [12] D. Khatamian, F.D. Manchester, The H–Y (Hydrogen-Yttrium) system, *Bulletin of Alloy Phase Diagrams* 9(3) (1988) 252-260.
- [13] A.P. Shivprasad, D.M. Frazer, V.K. Mehta, M.W.D. Cooper, T.A. Saleh, J.T. White, J.R. Wermer, E.P. Luther, D.V. Rao, Elastic moduli of high-density, sintered monoliths of yttrium dihydride, *Journal of Alloys and Compounds* 826 (2020) 153955.
- [14] A.A. Trofimov, X. Hu, H. Wang, Y. Yang, K.A. Terrani, Thermophysical properties and reversible phase transitions in yttrium hydride, *Journal of Nuclear Materials* 542 (2020) 152569.
- [15] J.C. Marshall, R. Van Houten, W.G. Baxter, 1000 Hour demonstration of clad yttrium hydride as a neutron moderator in: M. Ferrier (Ed.) *American Nuclear Society 1964 annual meeting*, American Nuclear Society, Inc., Philadelphia, 1964, p. 2.
- [16] M.N. Cinbiz, PLN-6268 Yttrium Hydride Post Irradiation Examination Plan, United States, 2022, p. Medium: ED.
- [17] L. Greenwood, Fluence Capsules for the LANL-MOD-1 Experiment, Pacific Northwest National Laboratory, PNNL-75643, 2020.
- [18] ASTM Standard Test Method for Measuring Fast-Neutron Reaction Rates by Radioactivation of Niobium, E1297, West Conshohocken, PA, 2018.
- [19] ASTM International. E1461-13 Standard Test Method for Thermal Diffusivity by the Flash Method, West Conshohocken, PA, 2013.
- [20] Netzsch Proteus Thermal Analysis Software, v. 7.2. Netzsch Instruments GmbH, 2019.